An AFC-stabilized implicit finite element method for partial differential equations on evolving-in-time surfaces

Andriy Sokolov, Ramzan Ali, Stefan Turek

Institut für Angewandte Mathematik, TU Dortmund
Vogelpothsweg 87
44227 Dortmund, Germany

Abstract

In this article we present a new implicit numerical scheme for reaction-diffusion-advection equations on an evolving in time hypersurface $\Gamma(t)$. The partial differential equations together with a level set equation ϕ are solved on a stationary quadrilateral mesh. The zero level set of the time dependent indicator function $\phi(t)$ implicitly describes the position of $\Gamma(t)$. The dominating convective-like terms, which are due to the presence of chemotaxis, transport of the cell density and surface evolution may lead to the non-positiveness of a given numerical scheme and in such a way cause appearance of negative values and give rise of nonphysical oscillations in the numerical solution. The proposed finite element method is constructed to avoid this problem: implicit treatment of corresponding discrete terms in combination with the algebraic flux correction (AFC) techniques make it possible to obtain a sufficiently accurate solution for reaction-diffusion-advection PDEs on evolving surfaces.

Keywords: level set, evolving surfaces, FEM, FCT, TVD, membrane, pattern-formation

1. Introduction

Current applications in biomathematics demand fast, efficient and accurate solvers for systems of reaction-diffusion-advection PDEs. For example, pattern formations and colouring of the animals coat [23, 24, 25, 39], dynam-

Email addresses: asokolow@math.tu-dortmund.de (Andriy Sokolov), rali@math.tu-dortmund.de (Ramzan Ali), ture@featflow.de (Stefan Turek)

ics of the yeast cell polarity [12, 29] and other processes are modeled by reaction-diffusion equations of Turing type instability. Chemotaxis models are widely used to describe bacteria/cell aggregation and formation processes [2, 22, 36, 37, 38], modeling of tumor invasion and metastasis processes before a proliferation dominated stage [5, 7, 8, 9, 10], modeling of vasculogenesis [4, 11, 30], etc. Here, besides diffusion and reaction one deals with the advection-like term which is due to specie-specie or specie-agent interactions.

During the last years there are tendencies to extend these mathematical models to more complex, but on the other hand more physically reasonable systems by coupling them with PDEs, which are defined on an evolving-in-time manifold $\Gamma(t)$, see, e.g., [1, 6, 13] for reaction-diffusion patterns on growing surfaces, [42, 41] for chemotaxis processes on stationary and deforming manifolds, [12, 29] for protein dynamics on a cell's membrane, etc. Mathematically, aforementioned physical models can be described by the following system of reaction-advection-diffusion equations

$$\frac{\partial c_i}{\partial t} = D_i^c \Delta c_i - \nabla \cdot [\chi_i^c \boldsymbol{w}_i^c(\boldsymbol{c}, \boldsymbol{\rho}) c_i] + f_i(\boldsymbol{c}, \boldsymbol{\rho}), \quad \text{in } \Omega \times T, \tag{1}$$

$$\frac{\partial^* \rho_j}{\partial t} = D_j^\rho \Delta_{\Gamma(t)} \rho_j - \nabla_{\Gamma(t)} \cdot (\chi_j^\rho \boldsymbol{w}_j^\rho(\boldsymbol{c}, \boldsymbol{\rho}) \rho_j) + g_j(\boldsymbol{c}, \boldsymbol{\rho}), \quad \text{on } \Gamma(t) \times (2)$$

where $\frac{\partial^* \rho_j}{\partial t}$ is a time-derivative, which takes into account the evolution of $\Gamma(t)$ and will be explained in the next section. The corresponding boundary and initial conditions have to be provided. Here, $c_i(\boldsymbol{x}, t)$, $i = 1 \dots n$, are defined in the whole domain Ω and are solutions of (1). Unknown functions $\rho_j(\boldsymbol{x}, t)$, $j = 1 \dots m$ live on the surface $\Gamma(t) \subset \Omega$ and are solutions of (2). We adopt the notation by writing vector fields in a bold letters, i.e., $\boldsymbol{c} = (c_1, \dots, c_n)^T$. The next sections are only dedicated to develop an efficient and accurate technique including examples for the solution of equations (2). The evolving surface $\Gamma(t)$ is aligned with prescribed level set function and its solution is extended to the neighborhood of the surface $\Omega_\epsilon(t)$. The position of $\Gamma(t)$ is prescribed implicitly by the zero level set of the time-dependent level set function $\phi(t)$, those values are either given analytically or found by solving the transport equation

$$\frac{\partial \phi}{\partial t} + \boldsymbol{v} \cdot \nabla \phi = 0, \tag{3}$$

where $\boldsymbol{v}$ is the velocity of the surface, which can be prescribed analytically, or $\boldsymbol{v}$ can also be determined through forces acting on the surface Γ, e.g. chemo-attractive, chemo-repulsive forces, bending surface etc. By

the proper choice of numbers of equations n and m, parameters D_i^c and D_j^ρ, chemotaxis/advection-related functions $\boldsymbol{\chi}_i^c$ and $\boldsymbol{v}_i^c$, as well as kinetic terms $f_i(\cdot)$ and $g_j(\cdot)$, one can easily obtain any of the models from the above presented references. In Figure 1, $\Omega_\epsilon(t)$ is an ϵ-band around $\Gamma(t)$, the domain of interest $\Omega = \Omega_{in} \cup \Omega_{out} \cup \Gamma$, where $\Gamma(t)$ is taken as a zero level set of ϕ. In a series of papers [33, 34, 35] the authors constructed a robust and efficient numerical scheme for chemotaxis problems in 2 and 3 spatial dimensions, in the case when $n = 2$ and $m = 1$. There, the FCT-TVD stabilization techniques, Newton-like solvers and coupled as well as decoupled approaches were analyzed, see also [32]. It was shown that the solver was able to deliver physically appropriate and accurate numerical solutions. Using the FCT method and the operator splitting technique one can extend the proposed framework to models with multi-species and multi-chemos. In the paper [31] we constructed a numerical scheme for the equation of the type (2) coupled with a chemotaxis system and the surface Γ was considered to be stationary. In this article we will propose a numerical scheme for solution of the partial differential equation of type (2) on the time dependent surface with $j = 1$. This method treats implicitly the arising advective terms and boundary integrals, which are due to the surface evolution, the transport and chemotaxis-processes solve via a robust, positivity-preserving finite element based TVD/FCT-stabilization technique.

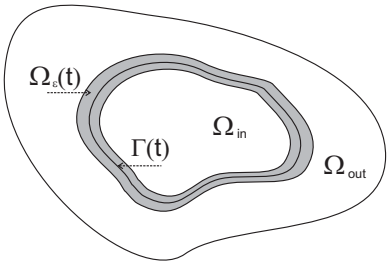

Figure 1: Geometrical illustration

The article is organized as follows: in section 2 we present the required theoretical derivations. Namely, in subsection 2.1 we explain the advective surface derivative and surface-related parameters, and in subsection 2.2 we describe the level set methodology and present the corresponding integral-theorems. Section 3 deals with the construction of an implicit numerical scheme, discuss the treatment of surface-advection and boundary-integral terms and discuss the corresponding stabilization techniques. In section 4 we present numerical results for reaction-diffusion partial differential equations in two spatial dimensions and examine the order of time- and space-convergence. Section 5 summarizes the characteristics of the proposed approach.

2. Theoretical results

2.1. Preliminaries and derivation

In this article we derive an implicit numerical scheme for the following parabolic chemotaxis-like equation on an evolving hypersurface $\Gamma(t)$

$$\frac{\partial^* \rho}{\partial t} = D\Delta_{\Gamma(t)}\rho - \nabla_{\Gamma(t)} \cdot (\chi\rho\nabla_{\Gamma(t)}c) + g(\rho) \ \text{ on } \ \Gamma(t) \times T, \tag{4}$$

which can be obtained from (2) by setting $j = 1$ and

$$\begin{aligned} D^\rho &= D, & \boldsymbol{\chi}^\rho &= \chi, \\ \boldsymbol{w}^\rho &= \nabla_{\Gamma(t)}c, & g(\boldsymbol{c}, \boldsymbol{\rho}) &= g(\rho). \end{aligned}$$

Here, the derivative

$$\frac{\partial^* \rho}{\partial t} = \partial_t^\bullet \rho + \rho\nabla_{\Gamma(t)} \cdot \boldsymbol{v} \tag{5}$$

is due to the evolution of $\Gamma(t)$ and can be obtained by the Leibniz formula

$$\frac{d}{dt}\int_{\Gamma(t)} \rho = \int_{\Gamma(t)} \partial_t^\bullet \rho + \rho\nabla_{\Gamma(t)} \cdot \boldsymbol{v}. \tag{6}$$

By $\partial_t^\bullet \rho = \partial_t \rho + \boldsymbol{v} \cdot \nabla\rho$ one denotes the advective surface material derivative. The surface velocity $\boldsymbol{v} = V\boldsymbol{n} + \boldsymbol{v}_S$ can be decomposed into velocity components in the normal direction $V\boldsymbol{n}$, with $\boldsymbol{n}$ to be a surface outward normal vector, and in the tangential direction $\boldsymbol{v}_S$. One can easily find that

$$V(\boldsymbol{x}, t) = -\frac{\phi_t(\boldsymbol{x}, t)}{|\nabla\phi(\boldsymbol{x}, t)|}.$$

Using the relations

$$\nabla_\Gamma \cdot \boldsymbol{v} = \nabla_\Gamma V \cdot \boldsymbol{n} + V\nabla_\Gamma \cdot \boldsymbol{n} + \nabla_\Gamma \cdot \boldsymbol{v}_S = V\nabla_\Gamma \cdot \boldsymbol{n} + \nabla_\Gamma \cdot \boldsymbol{v}_S = -VH + \nabla_\Gamma \cdot \boldsymbol{v}_S,$$

$$\boldsymbol{v} \cdot \nabla\rho = V\boldsymbol{n} \cdot \nabla\rho + \boldsymbol{v}_S \cdot \nabla\rho = V\frac{\partial\rho}{\partial\boldsymbol{n}} + \boldsymbol{v}_S \cdot \nabla\rho,$$

where H is a mean curvature, we can rewrite (4) as

$$\partial_t\rho + \boldsymbol{v}_S \cdot \nabla\rho - VH\rho + V\frac{\partial\rho}{\partial\boldsymbol{n}} + \rho\nabla_{\Gamma(t)} \cdot \boldsymbol{v}_S = D\Delta_{\Gamma(t)}\rho - \nabla_{\Gamma(t)} \cdot (\chi\rho\nabla_{\Gamma(t)}c) + g(\rho), \tag{7}$$

or, in terms of the surface material derivative, as

$$\partial_t^\bullet \rho + \rho\nabla_\Gamma \cdot \boldsymbol{v} = D\Delta_{\Gamma(t)}\rho - \nabla_{\Gamma(t)} \cdot (\chi\rho\nabla_{\Gamma(t)}c) + g(\rho). \tag{8}$$

2.2. Level set method

To obtain the semi-discrete form for equation (8) we adopt the level set method. We assume that $\Gamma(t) \subset \Omega$ is a compact smooth connected and oriented hypersurface in $\mathbb{R}^d$ and there exists a smooth level set function

$$\phi(t, \boldsymbol{x}) = \begin{cases} < 0 & \text{, if } \boldsymbol{x} \text{ is inside } \Gamma(t), \\ 0 & \text{, if } \boldsymbol{x} \in \Gamma(t), \\ > 0 & \text{, if } \boldsymbol{x} \text{ is outside } \Gamma(t), \end{cases} \tag{9}$$

such that $|\nabla\phi| \neq 0$. Then, an outward normal to $\Gamma(t)$ is

$$\boldsymbol{n} = (n_i)_i = \nabla\phi/|\nabla\phi| \tag{10}$$

and

$$\mathcal{P}_\Gamma = (\delta_{ij} - n_i n_j)_{ij} = I - \frac{\nabla\phi}{|\nabla\phi|} \otimes \frac{\nabla\phi}{|\nabla\phi|} \tag{11}$$

is the projection onto the tangent space $\mathcal{T}_{\boldsymbol{x}}\Gamma$. Observe that if $\phi(\cdot)$ is chosen as a signed distance function then $|\nabla\phi| = 1$. For a scalar function ξ on Ω and a tangential vector field $\boldsymbol{\xi}$ on Γ one obtains

$$\nabla_\Gamma \xi = \left(\frac{\partial \xi}{\partial x_i} - n_i n_j \frac{\partial \xi}{\partial x_j} \right)_i, \tag{12}$$

$$\nabla_\Gamma \cdot \boldsymbol{\xi} = \frac{\partial \xi_i}{\partial x_i} - n_i n_j \frac{\partial \xi_i}{\partial x_j}. \tag{13}$$

Therefore the Laplace-Beltrami operator on $\Gamma(t)$ with respect to the level set function ϕ can be written as

$$\Delta_\Gamma \xi = \nabla_\Gamma \cdot \nabla_\Gamma \xi = \nabla \cdot \mathcal{P}_\Gamma \nabla \xi. \tag{14}$$

The Eulerian mean curvature is defined through the level set function as

$$H = -\nabla \cdot \boldsymbol{n} = -\nabla \cdot \frac{\nabla\phi}{|\nabla\phi|}.$$

In the subsequent we will need the following lemmas.

Lemma 1. *(Coarea formula)*
Let for each $t \in [0, T]$, $\phi(t, \cdot) : \bar{\Omega} \to \mathbb{R}$ be Lipschitz continuous and assume that for each $r \in (inf_\Omega \phi, sup_\Omega \phi)$ the level set $\Gamma_r = \{x | \phi(x, \cdot) = r\}$ is a smooth d-dimensional hypersurface in $\mathbb{R}^{d+1}$. Suppose that $\eta : \bar{\Omega} \to \mathbb{R}$ is continuous and integrable. Then

$$\int_{inf_\Omega}^{sup_\Omega} \left(\int_{\Gamma_r} \eta \right) dr = \int_\Omega \eta |\nabla\phi|. \tag{15}$$

PROOF. Proof of the formula can be found [15].

Lemma 2. *(Eulerian integration by parts)*
Assume that the following quantities exist. Then, for a scalar function η and a vector field Q we have

$$\int_\Omega \nabla_{\Gamma(t)}\eta|\nabla\phi| = -\int_\Omega \eta H\boldsymbol{n}|\nabla\phi| + \int_{\partial\Omega}\eta(\boldsymbol{n}_{\partial\Omega} - \boldsymbol{n}\cdot\boldsymbol{n}_{\partial\Omega}\boldsymbol{n})|\nabla\phi|, \quad (16)$$

$$\int_\Omega \nabla_{\Gamma(t)}\cdot Q|\nabla\phi| = -\int_\Omega HQ\cdot\boldsymbol{n}|\nabla\phi| + \int_{\partial\Omega} Q\cdot(\boldsymbol{n}_{\partial\Omega} - \boldsymbol{n}\cdot\boldsymbol{n}_{\partial\Omega}\boldsymbol{n})|\nabla\phi|, \quad (17)$$

$$\begin{aligned}\int_\Omega \nabla_{\Gamma(t)}\cdot Q\eta|\nabla\phi| \quad &+ \quad \int_\Omega Q\cdot\nabla_{\Gamma(t)}\eta|\nabla\phi| = \\ -\int_\Omega Q\cdot\boldsymbol{n}\eta H|\nabla\phi| \quad &+ \quad \int_{\partial\Omega} Q\cdot(\boldsymbol{n}_{\partial\Omega} - \boldsymbol{n}\cdot\boldsymbol{n}_{\partial\Omega}\boldsymbol{n})\eta|\nabla\phi|, \end{aligned} \quad (18)$$

where $\boldsymbol{n}_{\partial\Omega}$ is an outward normal to $\partial\Omega$.

PROOF. For the proof see, e.g., [3].

Lemma 3. *(Implicit surface Leibniz formula)*
Let η be an arbitrary level set function defined on Ω such that the following quantities exist. Then

$$\frac{d}{dt}\int_\Omega \eta|\nabla\phi| = \int_\Omega (\partial_t^\bullet\eta + \eta\nabla_{\Gamma(t)}\cdot\boldsymbol{v})|\nabla\phi| - \int_{\partial\Omega}\eta\boldsymbol{v}\cdot\boldsymbol{n}_{\partial\Omega}|\nabla\phi|. \quad (19)$$

PROOF. For the proof see, e.g., [3].

Let us denote φ to be some test function, then using the coarea formula (15) we can write the variational formulation of (8):

$$\begin{aligned}\int_\Omega \left(\partial_t^\bullet\rho + \rho\nabla_\Gamma\cdot\boldsymbol{v}\right)\varphi|\nabla\phi| \quad &= \quad \int_\Omega \left(D\Delta_{\Gamma(t)}\rho - \nabla_{\Gamma(t)}\cdot(\chi\rho\nabla_{\Gamma(t)}c)\right)\varphi|\nabla\phi| \\ &+ \quad \int_\Omega g(\rho)\varphi|\nabla\phi|. \end{aligned} \quad (20)$$

Due to the implicit surface Leibniz formula (19) the left hand side of (20) can be rewritten as

$$\begin{aligned}\int_\Omega (\partial_t^\bullet\rho + \rho\nabla_{\Gamma(t)}\cdot\boldsymbol{v})\varphi|\nabla\phi| \quad &= \quad \frac{d}{dt}\int_\Omega \rho\varphi|\nabla\phi| \\ &- \quad \int_\Omega \rho\partial_t^\bullet\varphi|\nabla\phi| + \int_{\partial\Omega}\rho\varphi\boldsymbol{v}\cdot\boldsymbol{n}_{\partial\Omega}|\nabla\phi| \end{aligned} \quad (21)$$

In general the boundary integral cannot be neglected. In Section (4) we show that its non-inclusion into the numerical scheme can cause kinks and wiggles in the solution near boundaries which grow and spread throughout the domain as time evolves. Since $\big(D\nabla_{\Gamma(t)}\rho - \chi\rho\nabla_{\Gamma(t)}c\big)\cdot\boldsymbol{n} = 0$, integration by parts in (18) gives

$$\begin{aligned}
&\int_\Omega (D\nabla_{\Gamma(t)}\rho - \chi\rho\nabla_{\Gamma(t)}c)\cdot\nabla_{\Gamma(t)}\varphi|\nabla\phi| = \\
&-\int_\Omega \varphi\nabla_{\Gamma(t)}\cdot(D\nabla_{\Gamma(t)}\rho - \chi\rho\nabla_{\Gamma(t)}c)|\nabla\phi| \\
&+\int_{\partial\Omega} (D\nabla_{\Gamma(t)}\rho - \chi\rho\nabla_{\Gamma(t)}c)\cdot\boldsymbol{n}_{\partial\Omega}\varphi|\nabla\phi|. \qquad (22)
\end{aligned}$$

The boundary integral $\int_{\partial\Omega}(D\nabla_{\Gamma(t)}\rho - \chi\rho\nabla_{\Gamma(t)}c)\cdot\boldsymbol{n}_{\partial\Omega}\varphi|\nabla\phi|$ on the right hand side of (22) cannot be neglected in general as well. Its numerical treatment though can be performed in a similar way to the boundary integral $\int_{\partial\Omega}\rho\varphi\boldsymbol{v}\cdot\boldsymbol{n}_{\partial\Omega}|\nabla\phi|$ from (21). For the brevity everywhere in this article we assume that the boundary $\partial\Omega$ is aligned with some level set Γ_r and therefore $(D\nabla_{\Gamma(t)}\rho - \chi\rho\nabla_{\Gamma(t)}c)\cdot\boldsymbol{n}_{\partial\Omega} = 0$. Applying (21) and (22) to (20), we obtain

$$\begin{aligned}
&\frac{d}{dt}\int_\Omega \rho\varphi|\nabla\phi| + \int_\Omega (D\nabla_{\Gamma(t)}\rho - \chi\rho\nabla_{\Gamma(t)}c)\cdot\nabla_{\Gamma(t)}\varphi|\nabla\phi| = \\
&\int_\Omega \rho\partial_t^\bullet\varphi|\nabla\phi| - \int_{\partial\Omega}\rho\varphi\boldsymbol{v}\cdot\boldsymbol{n}_{\partial\Omega}|\nabla\phi| + \int_\Omega g(\rho)\varphi|\nabla\phi|. \qquad (23)
\end{aligned}$$

3. Numerical scheme

For the discretization in space we use time-independent (conforming) bilinear finite elements with the corresponding space of test functions $Q_h = \text{span}\{\varphi_1,\dots,\varphi_N\}$. Therefore

$$\dot{\varphi} = \boldsymbol{v}\cdot\nabla\varphi \qquad (24)$$

and the semi-discretization problem for (25) reads: find $P\in Q_h$ such that

$$\begin{aligned}
&\frac{d}{dt}\int_\Omega P\varphi|\nabla\phi| + \int_\Omega (D\nabla_{\Gamma(t)}P - \chi\rho\nabla_{\Gamma(t)}c)\cdot\nabla_{\Gamma(t)}\varphi|\nabla\phi| = \qquad (25)\\
&\int_\Omega P\boldsymbol{v}\cdot\nabla\varphi|\nabla\phi| - \int_{\partial\Omega}P\varphi\boldsymbol{v}\cdot\boldsymbol{n}_{\partial\Omega}|\nabla\phi| + \int_\Omega g(\rho)\varphi|\nabla\phi| \quad \forall\varphi\in Q_h.
\end{aligned}$$

The algorithm proposed by C. M. Elliott et al. [3] is the level set-based finite element method, where diffusive and advective terms are treated implicitly

but the surface-evolution term $\int_\Omega P\boldsymbol{v}\cdot\varphi|\nabla\phi|$ treated explicitly. This method has some interesting properties: First, stationary finite elements save time of calculation and reduce the complexity of a solver. Secondly, the level set nature makes it possible to couple surface-defined PDEs with the domain-defined PDEs. Additional prescription of a transport equation for the level set function can allow to model a complex behavior of the evolving in time hypersurface $\Gamma(t)$. And thirdly, the method does not require numerical evaluation of the curvature. Nevertheless, for more practical use this method has to be improved because of a few drawbacks. On the one hand, this method does not include any stabilization for the convective term, which is due to the surface evolution in time, and which may cause the numerical scheme to loose its positivity-preserving properties and thus lead to oscillatory solutions with negative values. On the other hand, this method does not include integral-boundary terms. Under some conditions the absence of corresponding discrete terms in the numerical scheme may lead to the loss of accuracy of the solution near boundaries. This may also cause loss of positivity of the solution near boundaries follows by deterioration of the entire solution. To overcome these stumbling-blocks, we adopted a fully implicit FCT/TVD-stabilized finite element method inclusive boundary integrals.

Fully-discrete scheme of the implicit version: Given P^m at the t^m-the time instance and the time step $\Delta t = t^{m+1} - t^m$, then solve for P^{m+1}

$$\begin{aligned}
&\frac{1}{\Delta t}\int_\Omega P^{m+1}\varphi|\nabla\phi^{m+1}| + \int_\Omega (D\nabla_{\Gamma^{m+1}}P^{m+1} - \boldsymbol{w}P^{m+1})\cdot\nabla_{\Gamma^{m+1}}\varphi|\nabla\phi^{m+1}| \\
&- \int_\Omega P^{m+1}\boldsymbol{v}^{m+1}\cdot\nabla\varphi|\nabla\phi^{m+1}| + \int_{\partial\Omega} P^{m+1}\varphi\boldsymbol{v}^{m+1}\cdot\boldsymbol{n}_{\partial\Omega}|\nabla\phi^{m+1}| \\
&= \frac{1}{\Delta t}\int_\Omega P^m\varphi|\nabla\phi^m + \int_\Omega g\varphi|\nabla\phi^m|, \qquad (26)
\end{aligned}$$

for all $\varphi \in S_h$. Using $\{\varphi_i\}$ test functions as quadrilateral finite elements in space, the matrix form of the equation (26) looks like follows:

$$\begin{aligned}
[\boldsymbol{M}(|\nabla\phi^{m+1}|) \;&+\; \Delta t\boldsymbol{L}(D|\nabla\phi^{m+1}|) - \Delta t\boldsymbol{K}(\boldsymbol{w}^m|\nabla\phi^{m+1}|) \\
&-\; \Delta t\boldsymbol{N}(\boldsymbol{v}^{m+1}|\nabla\phi^{m+1}|) + \Delta t\boldsymbol{R}(|\nabla\phi^{m+1}|)]\,P^{m+1} \\
&= \boldsymbol{M}(|\nabla\phi^m|)P^m + \Delta t g(|\nabla\phi^m|) \qquad (27)
\end{aligned}$$

Here, $\boldsymbol{M}(\cdot)$ denotes the (consistent) mass matrix, $\boldsymbol{L}(\cdot)$ is the discrete Laplace-Beltrami operator, $\boldsymbol{K}(\cdot)$ is the discrete on-surface advection operator with

the linearized velocity $\boldsymbol{w}^m$, $\boldsymbol{N}(\cdot)$ is the discrete operator due to the surface evolution and $\boldsymbol{R}(\cdot)$ are discrete boundary integrals with the entries defined by the formulae

$$m_{ij}(\psi) = \int_\Omega \varphi_i \varphi_j \psi, \tag{28}$$

$$l_{ij}(\psi) = \int_\Omega P_\Gamma \nabla \varphi_i \cdot \nabla \varphi_j \psi, \tag{29}$$

$$k_{ij}(\boldsymbol{\psi}) = \int_\Omega \varphi_i \boldsymbol{\psi} \cdot P_\Gamma \varphi_j, \tag{30}$$

$$n_{ij}(\boldsymbol{\psi}) = \int_\Omega \varphi_i \boldsymbol{v}^{m+1} \cdot \nabla \varphi_j \boldsymbol{\psi}, \tag{31}$$

$$g_i(\psi) = \int_\Omega \varphi_i g_i \psi. \tag{32}$$

It is known that under some conditions the discrete Laplace-Beltrami operator $\boldsymbol{L}(D|\nabla\phi|)$ can deteriorate and leads to an ill-conditioned matrix. In this article we do not investigate this situation and refer to the corresponding works of Olshanskii *et al.* [26, 27, 28]. The convective-like matrices $\boldsymbol{K}(\cdot)$ and $\boldsymbol{N}(\cdot)$ depending on velocities $\boldsymbol{w}$ and $\boldsymbol{v}$, as well as the boundary-integral operator $\boldsymbol{R}(\cdot)$ may lead to the loss the positivity-preserving properties and thus lead to nonphysical oscillations in the solution profile. This fact necessitates the use of some stabilization based techniques to treat the operators or terms which caused oscillation. Rewriting the equation (27) as

$$\begin{aligned}[\boldsymbol{M}(|\nabla\phi^{m+1}|) &+ \Delta t \boldsymbol{L}(D|\nabla\phi^{m+1}|) - \Delta t \boldsymbol{\mathcal{K}}(\phi^{m+1}|) \\ &= \boldsymbol{M}(|\nabla\phi^m|)P^m + \Delta t g(|\nabla\phi^m|)\end{aligned} \tag{33}$$

we apply the linearized flux-corrected transport (FCT) algorithm to the operator

$$\boldsymbol{\mathcal{K}}(\phi^{m+1}|) = \boldsymbol{K}(\boldsymbol{w}^m|\nabla\phi^{m+1}|) - \Delta t \boldsymbol{N}(\boldsymbol{v}^{m+1}|\nabla\phi^{m+1}|) + \Delta t \boldsymbol{R}(|\nabla\phi^{m+1}|).$$

Positivity constraints are enforced using a nonlinear blend of high- and low-order approximations through an algebraic manipulation of the matrices $\boldsymbol{M}$ and $\boldsymbol{\mathcal{K}}$. The limiting strategy is fully multidimensional and applicable to (multi-)linear finite element discretizations on unstructured meshes. The approach was successfully tested for domain-defined equations for chemotaxis in 2- and 3-spatial dimensions [33, 34] and for chemotaxis equations which are defined on stationary surfaces [31]. For a detailed presentation of the FEM-FCT methodology, including theoretical analysis (stability, positivity, convergence) and technical implementation details (data structures,

matrix assembly) we refer the interested reader to [16, 17, 18, 19, 20] and other related publications of Kuzmin *et al.*

4. Numerical results

4.1. Example 1

In the first example we would like to demonstrate that numerical stabilization of certain PDEs on surfaces is necessary. For these purposes we consider the transport equation

$$\partial_t \rho + \boldsymbol{v} \cdot \nabla_\Gamma \rho = 0 \tag{34}$$

on the unit sphere $\Gamma = \{\boldsymbol{x} : |\boldsymbol{x}| = 1\}$. Applying the level set methodology, we solve the transport equation (34) on level sets $\Gamma_c \subset \Omega$. For the sake of simplicity our calculational domain Ω is chosen to be a union of all level sets Γ_c with $c \in [0.5, 1.5]$. The following initial condition

$$\rho(\boldsymbol{x}, t) = \begin{cases} 10 & \text{if } |\boldsymbol{x} - (0,0,1)^T| \leq 0.3\ , \\ 0 & \text{else.} \end{cases} \tag{35}$$

and the advective velocity vector-field

$$\boldsymbol{v} = \{x_1, 0, -x_3\}^T$$

are taken. The mesh is constructed by refining the coarsest level via connecting opposite midpoints several times. In the table below we give the number of cells and degrees of freedom at every level of refinement. For numerical experiments we use a grid of trilinear finite elements at the 5th level of mesh refinement. Edges of quadrilaterals are aligned with the level sets. Figure 2(a) we show the initial condition for ρ. Its numerical solution for the pure Galerkin scheme at an exemplary time-point $T = 0.2$ is demonstrated in Figure 2(b). One can clearly observe artificial wiggles and negative values of ρ near regions of steep gradients. These nonphysical negative

level	cells	d.o.f.
1	192	250
2	1 536	1 746
3	12 288	13 090
4	98 304	101 442
5	786 432	798 850

Table 1: Mesh levels on the computational domain Ω.

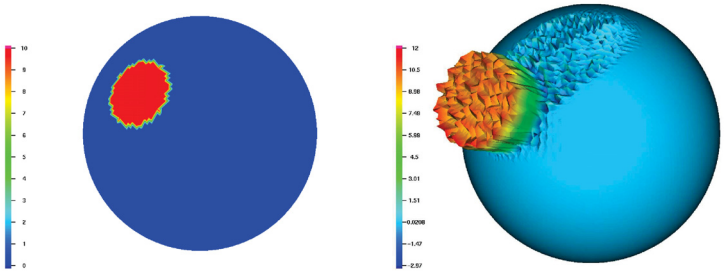

(a) initial solution

(b) pure Galerkin method

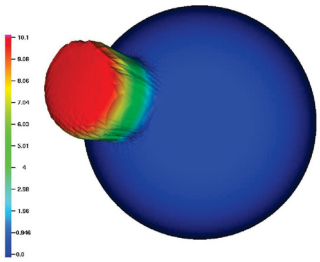

(c) TVD

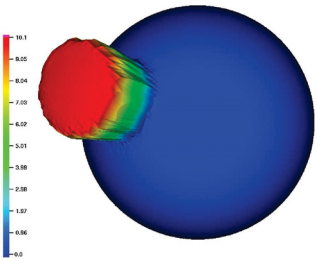

(d) FCT

Figure 2: Numerical results for the transport problem, $\Delta t = 0.001$.

values grow rapidly as time evolves, which leads to an abnormal termination of the simulation run. In [31] we also showed that the pure Galerkin scheme for chemotaxis problems on stationary surfaces cannot guarantee positivity preservation and smoothness of the solution. The corresponding FCT/TVD methodology helps to stabilize this type of problems and delivers a sufficiently accurate solution, see Figures 2(c) and 2(d) as well as [31]. In the following we show that the integral boundary term $\int_{\partial\Omega} \rho\varphi \boldsymbol{v} \cdot \boldsymbol{n}_{\partial\Omega} |\nabla\phi|$ can also lead to undesired kinks near the boundary of the calculation domain, which can also spread through the whole domain and spoil the numerical solution. An advective term to the surface evolution requires the special numerical treatment as well. For corresponding reconstruction processes we refer, e.g., to [21].

4.2. Example 2

Let us take example 1 from [3]. We solve the following equation

$$\frac{\partial^* \rho(\boldsymbol{x},t)}{\partial t} = D\Delta_{\Gamma(t)}\rho(\boldsymbol{x},t) + g(\boldsymbol{x},t) \qquad \text{on} \quad \Gamma(t), \tag{36}$$

where $\Gamma(t)$ is prescribed by the zero level set of the function

$$\phi(\boldsymbol{x},t) = |\boldsymbol{x}| - 1.0 + \sin(4\,t)(|\boldsymbol{x}| - 0.5)(1.5 - |\boldsymbol{x}|). \tag{37}$$

As a domain we choose $\Omega = \{\boldsymbol{x} \in \mathbb{R}^2 : 0.5 \leq |\boldsymbol{x}| \leq 1.5\}$. The boundary of the domain $\partial\Omega$ is aligned with a curve from the family Γ_r. The analytical solution is chosen to be

$$\rho(\boldsymbol{x},t) = e^{-t/|\boldsymbol{x}|^2}\frac{x_1}{|\boldsymbol{x}|^2}.$$

Since $\Gamma(t)$ is time-dependent, the equation (36) transforms into

$$\partial_t\rho + \boldsymbol{v}_S \cdot \nabla\rho + V\frac{\partial\rho}{\partial\boldsymbol{n}} - VH\rho + \rho\nabla_\Gamma \cdot \boldsymbol{v}_S - \Delta_\Gamma\rho = g, \tag{38}$$

where H is a mean curvature of $\Gamma(t)$ and therefore $H = -1/|\boldsymbol{x}|$. Substituting $v_S = 0$ into (38) we get

$$\partial_t\rho + V\frac{\partial\rho}{\partial\boldsymbol{n}} - VH\rho - \Delta_\Gamma\rho = g. \tag{39}$$

The function $\rho(\boldsymbol{x},t)$ from (4.2) solves

$$\partial_t\rho - \Delta_\Gamma\rho = 0.$$

Therefore, one finds that

$$g = V\frac{\partial\rho}{\partial\boldsymbol{n}} - VH\rho = V\rho\left(\frac{2\,t}{|\boldsymbol{x}|^3} + \frac{1}{|\boldsymbol{x}|}\right).$$

As the initial condition we set $\rho_{\text{init}} = \rho(\boldsymbol{x}, t = 0)$. In figures 3(c) and 3(d) we demonstrate numerical results after the 1000th iteration with the fixed time step $\Delta t = 0.0001$ obtained by a scheme, which does not include a boundary integral term. Here, explicit and implicit schemes reveal the same artifact in the numerical solution: artificial kinks near the outside boundary of the domain might propagate in time to the whole domain causing deterioration of the numerical solution. In figures 4(a), 4(b) and 4(c) we show numerical solutions, which are obtained by the implicit scheme (26). One can clearly see much better profiles of the numerical solution. The 3rd level of the mesh

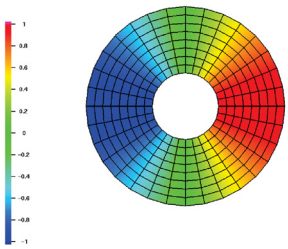

(a) mesh at level 2 and initial solution

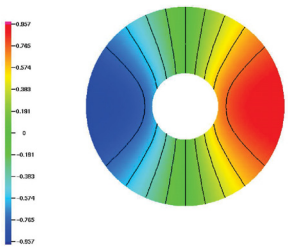

(b) analytical solution

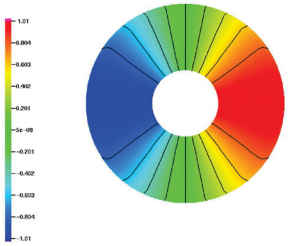

(c) numerical solution, level 3

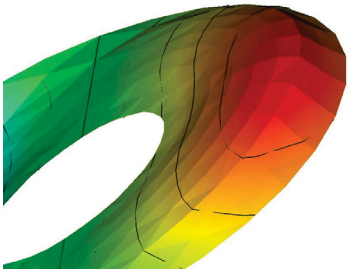

(d) boundary kinks, level 2

Figure 3: The 2nd and 3rd levels of mesh refinement consists of 288 and 1088 degrees of freedom respectively.

refinement is used. In figure 4(a) we demonstrate the numerical solution of (26) without any stabilization. In figure 4(a) the TVD and in figure 4(c) the FCT stabilization techniques are applied. In the corresponding tables we show the $L_2(\Omega_\epsilon)$, and $H_1(\Omega_\epsilon)$-errors which are defined by

$$L_2(\Omega_\epsilon)\text{-error} = \frac{\|\rho_{\text{analytical}}(\boldsymbol{x},t) - \rho_{\text{numerical}}(\boldsymbol{x},t)\|_{L_2(\Omega_\epsilon)}}{\text{Area}\,(\Omega_\epsilon)},$$

$$H_1(\Omega_\epsilon)\text{-error} = \frac{\|\nabla(\rho_{\text{analytical}}(\boldsymbol{x},t) - \rho_{\text{numerical}}(\boldsymbol{x},t))\|_{L_2(\Omega_\epsilon)}}{\text{Area}\,(\Omega_\epsilon)}.$$

In the upcoming tables the $L_2(\Omega_\epsilon)$-errors, order of convergence and numbers of degrees of freedom are calculated at 1000th time step. Table 2 is constructed in the whole domain without and with TVD/FCT stabilization techniques, respectively.

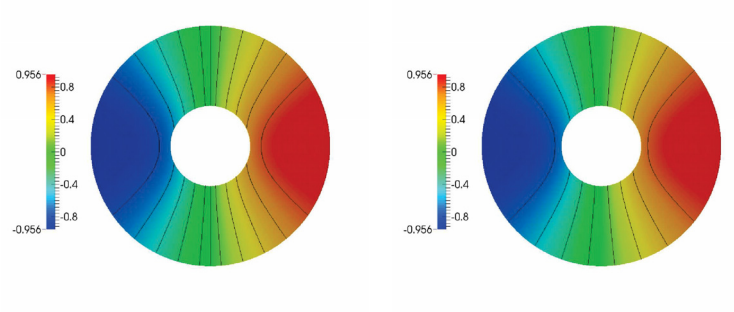

(a) Implicit scheme without stabilization

(b) Implicit scheme with TVD stabilization

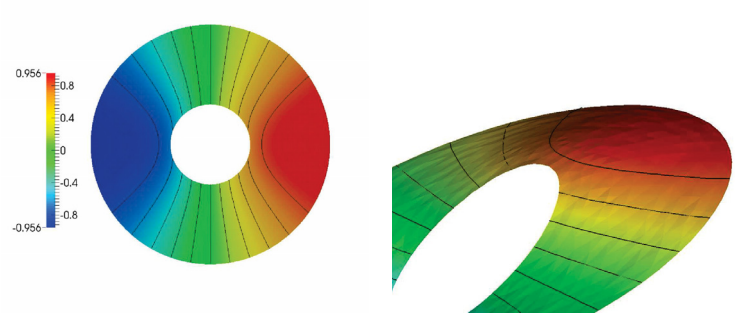

(c) Implicit scheme with FCT stabilization

(d) no boundary kinks

Figure 4: Numerical solutions obtained by adoption of the fully implicit scheme (26).

lev.	d.o.f	$L_2(\Omega_\epsilon)$ -errors	order	$H_1(\Omega_\epsilon)$ -errors	order
Including boundary integral without stabilization					
2	288	3.32928E-003	–	3.38593E-002	–
3	1088	1.25199E-003	1.4110	2.35593E-002	0.5233
4	4224	4.55928E-004	1.4574	1.66758E-002	0.4985
5	16640	1.69121E-004	1.4307	1.23715E-002	0.4307
6	66048	5.97876E-005	1.5001	9.05951E-003	0.4495
Total variation diminishing (TVD) schemes					
2	288	3.72731E-003	–	3.34255E-002	–
3	1088	1.33463E-003	1.4817	2.27460E-002	0.5553
4	4224	4.70020E-004	1.5057	1.59574E-002	0.5114
5	16640	1.70923E-004	1.4594	1.18479E-002	0.4296
6	66048	5.98328E-005	1.5143	8.69003E-003	0.4472
Flux Corrected Transport (FCT) schemes					
2	288	3.34406E-003	–	3.37376E-002	–
3	1088	1.25317E-003	1.4160	2.35129E-002	0.5209
4	4224	4.56032E-004	1.4584	1.66585E-002	0.4972
5	16640	1.69131E-004	1.4310	1.23644E-002	0.4301
6	66048	5.97813E-005	1.5004	9.05490E-003	0.4494

Table 2: $L_2(\Omega_\epsilon)$ and $H_1(\Omega_\epsilon)$-errors, numbers of degrees of freedom and orders are calculated in the domain $\Omega_{\text{in}} \cup \Omega_{\text{out}}$

4.3. *Example 3*

As a 3rd test case we take example 2 from [3]: we solve the equation (36) in the domain $\Omega = \{\boldsymbol{x} \in \mathbb{R}^2 : 0.5 \leq |\boldsymbol{x}| \leq 1.5\}$ on stationary level sets

$$\phi(\boldsymbol{x}, t) = |\boldsymbol{x}| - 1.0.$$

Here, the initial solution is $\rho_0(\boldsymbol{x}) = \sin(4\gamma)$ and the tangential velocity of the surface Γ is $\boldsymbol{v}_S = 0$. Since $\gamma_t = 0$, the normal component of the surface velocity V is also zero. The mean value of ρ_0 vanishes on every level set Γ_r, hence the solution tends to zero as time tends to infinity. Obtained numerical solutions at successive time instances are presented in figure 5.

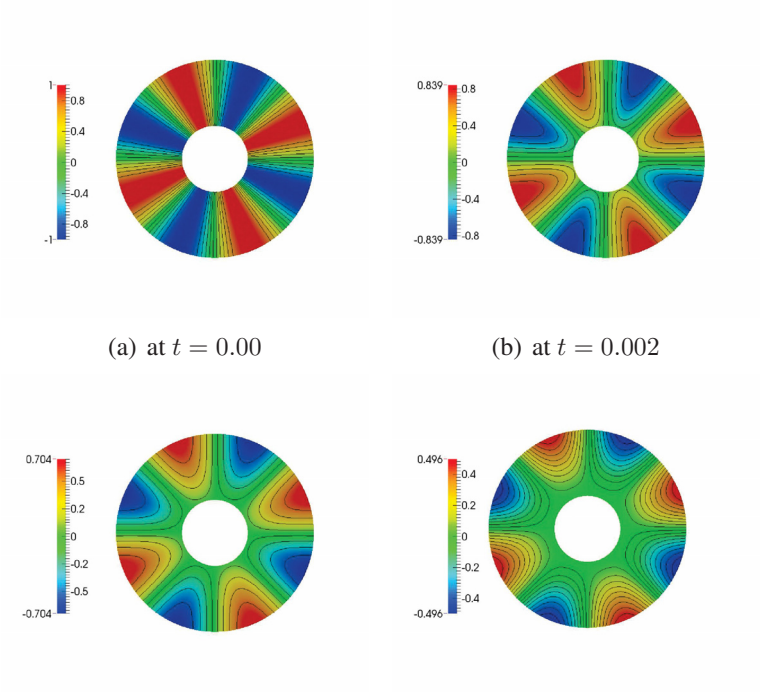

(a) at $t = 0.00$ (b) at $t = 0.002$

(c) at $t = 0.045$ (d) at $t = 0.1$

Figure 5: Solution of example 3 at various time instances, $\Delta t = 0.0001$

lev.	d.o.f	$L_2(\Omega_\epsilon)$ -errors	order	$H_1(\Omega_\epsilon)$ -errors	order
Including boundary integral without stabilization					
2	288	6.65856E-003	–	6.77186E-002	–
3	1088	2.50399E-003	1.4110	4.71187E-002	0.5532
4	4224	9.11856E-004	1.5092	3.33517E-002	0.5151
5	16640	3.38243E-004	1.5130	2.47431E-002	0.4844
6	66048	1.19575E-004	1.5001	1.81190E-002	0.4495
Total variation diminishing (TVD) schemes					
2	288	7.45463E-003	–	6.68511E-002	–
3	1088	2.66927E-003	1.4817	4.54921E-002	0.5553
4	4224	9.40041E-004	1.5056	3.19149E-002	0.5114
5	16640	3.41847E-004	1.4594	2.36959E-002	0.4296
6	66048	1.19665E-004	1.5143	1.73800E-002	0.4472
Flux Corrected Transport (FCT) schemes					
2	288	6.68813E-003	–	6.74752E-002	–
3	1088	2.50635E-003	1.4110	4.70259E-002	0.5532
4	4224	9.12065E-004	1.5092	3.33171E-002	0.5151
5	16640	3.38263E-004	1.5130	2.47289E-002	0.4844
6	66048	1.19562E-004	1.5004	1.81098E-002	0.4494

Table 3: $L_2(\Omega_\epsilon)$ and $H_1(\Omega_\epsilon)$ errors and order of convergence and number of degrees of freedom in the band $0.75 < |\boldsymbol{x}| < 1.25$

4.4. Example 4

Now everything is similar to the previous example 4.3, but the tangential velocity of the surface is defined as

$$\boldsymbol{v}_S = 10\frac{(-\phi_{x_2}, \phi_{x_1})}{|\nabla\phi|}. \tag{40}$$

Numerical results at some instances of time intervals are shown in figure 6.
In Tables 3 and 4 we show the $L_2(\Omega_\epsilon)$ and $H_1(\Omega_\epsilon)$ errors with order of convergence and number of degrees of freedom with different mesh refinement levels on the stripes $0.75 < |\boldsymbol{x}| < 1.25$ and $0.85 < |\boldsymbol{x}| < 1.15$, respectively.

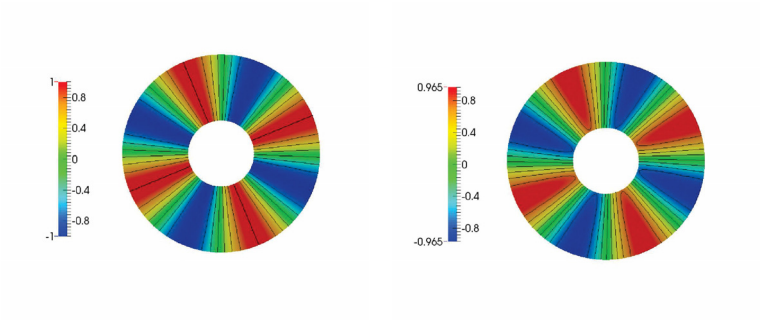

(a) at $t = 0.0$ (b) at $t = 0.002$

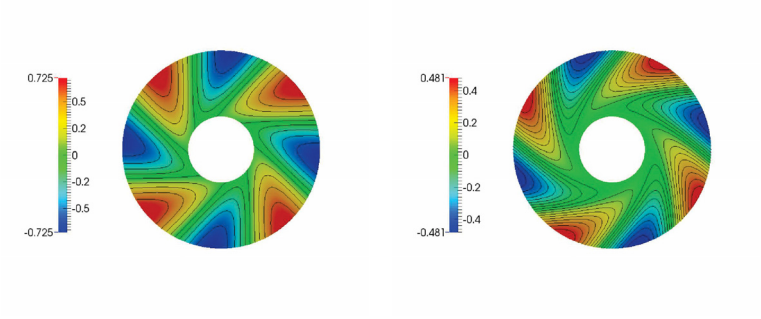

(c) at $t = 0.045$ (d) at $t = 0.1$

Figure 6: Solution of example 4 at various time instances, $\Delta t = 0.0001$

lev.	d.o.f	$L_2(\Omega_\epsilon)$ -errors	order	$H_1(\Omega_\epsilon)$ -errors	order
Including boundary integral without stabilization					
2	288	1.10976E-002	–	1.12864E-001	–
3	1088	4.17333E-003	1.4110	7.85311E-002	0.5232
4	4224	1.51976E-003	1.4574	5.55863E-002	0.4985
5	16640	5.63739E-004	1.4307	4.12386E-002	0.4307
6	66048	1.99292E-004	1.5001	3.01983E-002	0.4495
Total variation diminishing (TVD) schemes					
2	288	1.24243E-002	–	1.11418E-001	–
3	1088	4.44879E-003	1.4817	7.58203E-002	0.5553
4	4224	1.56673E-003	1.5057	5.31915E-002	0.5113
5	16640	5.69745E-004	1.4594	3.94932E-002	0.4295
6	66048	1.99442E-004	1.5143	2.89667E-002	0.4472
Flux Corrected Transport (FCT) schemes					
2	288	1.11468E-002	–	1.12458E-001	–
3	1088	4.17726E-003	1.4160	7.83766E-002	0.5209
4	4224	1.52010E-003	1.4584	5.55285E-002	0.4971
5	16640	5.63772E-004	1.4310	4.12149E-002	0.4300
6	66048	1.99271E-004	1.5004	3.01830E-002	0.4494

Table 4: $L_2(\Omega_\epsilon)$ and $H_1(\Omega_\epsilon)$ errors and orders in the strip $0.85 < |\boldsymbol{x}| < 1.15$

5. Conclusion

Modern biological and medical applications require numerical solutions of systems of partial differential equations (PDEs) on manifolds/surfaces and their coupling with domain-defined PDEs. The level set methodology largely allows for such a coupling by a surface-surrounding bulk and provides the mathematical machinery for the development of numerical methods for PDEs on closed manifolds. Substantial difficulties occur when the surface and its corresponding level set function are time dependent, i.e., non-stationary. Here, one does not only have to carefully treat additional terms which arise due to the surface evolution, but also has to come up with a robust stabilization for advective terms which are caused by deformations of the surface, chemotaxis effects, advective surface material derivatives, boundary integrals, etc. In this article we proposed a fully implicit numerical scheme for systems of reaction-diffusion-convection/chemotaxis equations on an evolving in time surface. The positivity preservation is guaranteed by the TVD/FCT stabilization technique. The presented numerical results show a sufficient accuracy, given a domain $\Omega \subset \mathbb{R}^2$. The employed mathematical techniques such as the level set method, finite element discretization in space and TVD/FCT stabilization of advective terms provide a straightforward extension of a given method to the 3-dimensional space with an embedded 2-dimensional hypersurface. Next steps will be to implement and comprehensively study the given method in 3D in order to verify its merits for more complex bio-medical applications. The proposed numerical scheme was implemented in the open source FEM-library FEAT2, which is developed and maintained at the department of Mathematics at the TU Dortmund. The downloading of this software and the corresponding tutoring is possible either from `www.featflow.de` or by writing an email to one of the authors of the article.

Acknowledgments

Ramzan Ali is supported through faculty development program from "University of Central Asia" in collaboration with "DAAD".

[1] R. Barreira, C. M. Elliott and A. Madzvamuse, The surface finite element method for pattern formation on evolving biological surfaces. Journal of Mathematical Biology, **63**, no. 6 (2011), 1095–1119.

[2] (MR2269589) M. Aida, T. Tsujikawa, M. Efendiev, A. Yagi and M. Mimura, *Lower estimate of the attractor dimension for a chemotaxis growth system*, J. London Math. Soc., **74**, no. 2 (2006), 453–474.

[3] G. Dziuk, C.M. Elliott, *An Eulerian approach to transport and diffusion on evolving implicit surfaces*, Comput Visual Sci, **13**, (2010), 17–28.

[4] (MR2157640) D. Ambrosi, F. Bussolino, L. Preziosi, *A review of vasculogenesis models*, Computational and Mathematical Methods in Medicine: An Interdisciplinary Journal of Mathematical, Theoretical and Clinical Aspects of Medicine, **6**, no. 1 (2005), 1–19.

[5] () A. R. A. Anderson, M A. J. Chaplain, E. L. Newman, R. J. C. Steele and A. M. Thompson, *Mathematical modelling of tumour invasion and metastasis*, Journal of Theoretical Medicine **2** (1999), 129–154.

[6] (MR2684158) M. Bergdorf, I. F. Sbalzarini, P. Koumoutsakos, *A Lagrangian particle method for reaction-diffusion systems on deforming surfaces*, J. Math. Biol., **61**, no. 5 (2009), 649–663.

[7] M. A. J. Chaplain, *The mathematical modelling of tumour angiogenesis and invasion*, ACTA Biotheoretica, **43**, no. 4 (1995), 387–402.

[8] M. A. J. Chaplain, *Continuous and discrete mathematical models of tumor-induced angiogenesis*, Bulletin of Mathematical Biology, **60** (1998), 857–900.

[9] M. A. J. Chaplain, *Mathematical modelling of angiogenesis*, Journal of Neuro-Oncology, **50** (2000), 37–51.

[10] M. A. J. Chaplain, A. M. Stuart, *A model mechanism for the chemotactic response of endothelial cells to tumour angiogenesis factor*, IMA Journal of Mathematics Applied in Medicine and Biology, **10** (1993), 149–168.

[11] A. Gamba, D. Ambrosi, A. Coniglio, A. de Candia, S. Di Talia, E. Giraudo, G. Serini, L. Preziosi, and F. Bussolino, *Percolation, morphogenesis, and Burgers dynamics in blood vessels formation*, Phys. Rev. Lett., **90** (2003).

[12] A. B. Goryachev and A. V. Pokhilko, *Dynamics of Cdc42 network embodies a Turing-type mechanism of yeast cell polarity*, FEBS Lett **582**, no. 10, pp. 1437–1443, 2008.

[13] G. Hetzer, A. Madzvamuse and W. Shen *Characterization of Turing diffusion-driven instability on evolving domains*, Discrete and Continuous Dynamical Systems - Series A, **32**, no. 11 (2012), 3975–4000.

[14] L. Tian, C. B. Macdonald, and S. J. Ruuth, *Segmentation on surfaces with the closest point method*, , Int Conf on Image Processing, Cairo, Egypt, **ICIP09** (2009).

[15] I. Chavel *Riemannian Geometry: A Modern Introduction* , Cambridge Studies in Advanced Mathematics, Cambridge University Press (1995).

[16] [978-94-077-4037-2] D. Kuzmin, R. Löhner and S. Turek, *Flux-Corrected Transport*, Springer, 2nd edition, 2012.

[17] (MR2129255) D. Kuzmin and M. Möller, *Algebraic flux correction I. Scalar conservation laws*, in "Flux-Corrected Transport: Principles, Algorithms, and Applications" (Eds. D. Kuzmin, R. Löhner, S. Turek), Springer, Berlin (2005), 155–206.

[18] (MR1880117) D. Kuzmin and S. Turek, *Flux correction tools for finite elements*, J. Comput. Phys., **175** (2002), 525–558.

[19] (MR2501695) D. Kuzmin, *Explicit and implicit FEM-TVD algorithms with flux linearization*, J. Comput. Phys., **228** (2009), 2517–2534.

[20] (MR2879702) D. Kuzmin, *Linearity-preserving flux correction and convergence acceleration for constrained Galerkin schemes*, Journal of Computational and Applied Mathematics, **236** (2012), 2317–2337.

[21] S. Turek, O. Mierka, S. Hysing and D. Kuzmin, *Numerical Study of a High Order 3D FEM-Level Set Approach for Immiscible Flow Simulation Numerical Methods for Differential Equations, Optimization, and Technological Problems*, Computational Methods in Applied Sciences, **27** (2013), 65–91.

[22] M. Mimura and T. Tsujikawa, *Aggregating pattern dynamics in a chemotaxis model including growth*, Physica A, **230** (1996), 499–543.

[23] (MR1687391) J. D. Murray, *Discussion: Turing's theory of morphogenesisIts influence on modelling biological pattern and form*, Bull. Math. Biol., **52** (1990), 119–152.

[24] J. D. Murray, *Mathematical Biology I: An Introduction*, Springer Verlag, Third Edition (2002).

[25] J. D. Murray, *Mathematical Biology II: Spatial Models and Biomedical Applications*, Springer Verlag, (2003).

[26] M. A. Olshanskii, A. Reusken and J. Grande, *A Finite Element method for elliptic equations on surfaces*, SIAM J. Numer. Anal. **47**, no. 5 (2009), pp. 3339-3358.

[27] M. A. Olshanskii, A. Reusken and X. Xu, *An Eulerian space-time Finite Element method for diffusion problems on evolving surfaces*, submitted to SINUM (2013).

[28] M. A. Olshanskii and A. Reusken, *Error analysis of a space-time finite element method for solving PDEs on evolving surfaces*, submitted to SINUM (2013).

[29] A. Rötz, M. Räger, *Turing Instabilities in a Mathematical Model for Signaling Networks*, Journal of Mathematical Biology, **65**, Issue 6-7 (2012), 1215–1244.

[30] G. Serini, D. Ambrosi, E. Giraudo, A. Gamba, L. Preziosi and F. Bussolino, *Modeling the early stages of vascular network assembly*, The EMBO Journal, **22** (2003), 1771–1779.

[31] A. Sokolov, R. Strehl and S. Turek, *Numerical simulation of chemotaxis models on stationary surfaces*, Discrete and Continuous Dynamical Systems, Series B, **18**, no. 10 (2013), 2689.

[32] R. Strehl, *Advanced numerical treatment of chemotaxis driven PDEs in mathematical biology*, Phd thesis, TU Dortmund (2013).

[33] (MR2770292) R. Strehl, A. Sokolov, D. Kuzmin and S. Turek, *A flux-corrected finite element method for chemotaxis problems*, Computational methods in applied mathematics, **10**, no. 2 (2010), 219–232.

[34] (MR2991973) R. Strehl, A. Sokolov, D. Kuzmin, D. Horstmann and S. Turek, *A positivity-preserving finite element method for chemotaxis problems in 3D*, Journal of Computational and Applied Mathematics, **239** (2013), 290–303.

[35] (MR2944801) R. Strehl, A. Sokolov and S. Turek, *Efficient, accurate and flexible Finite Element solvers for Chemotaxis problems*, Computers and Mathematics with Applications, **34**, no. 3 (2011), 175–189.

[36] R. Tyson, S. R. Lubkin and J. D. Murray, *A minimal mechanism for bacterial pattern formation*, Proc. R. Soc. Lond. B, **266** (1999), 299–304.

[37] (MR1687391) R. Tyson, S. R. Lubkin and J. D. Murray, *Model and analysis of chemotactic bacterial patterns in a liquid medium*, J. Math. Biol., **38** (1999), 359–375.

[38] (MR1803855) R. Tyson, L. G. Stern and R. J. LeVeque, *Fractional step methods applied to a chemotaxis model*, J. Math. Biol., **41** (2000), 455–475.

[39] V. K. Vanag and I. R. Epstein, *Pattern formation mechanisms in reaction-diffusion systems*, Int. J. Dev. Biol. **53**, no. (5-6) (2009), 673–81.

[40] B. Dong, *Applications of Variational Models and Partial Differential Equations in Medical Image and Surface Processing*, PhD theis, UCLA (2009).

[41] C. M. Elliott, B. Stinner and C. Venkataraman, *Modelling cell motility and chemotaxis with evolving surface finite elements*, J. R. Soc. Interface, PMID: 22675164, 2012.

[42] C. Landsberg, F. Stenger, A. Deutsch, M. Gelinsky, A. Rösen-Wolff and A. Voigt, *Chemotaxis of mesenchymal stem cells within 3D biomimetic scaffolds–a modeling approach*, J. Biomech., **44**, no. 2 (2011), 359–364.